PNAS RESEARCH ARTICLE | NEUROSCIENCE

The endocannabinoid 2-arachidonoylglycerol is released and transported on demand via extracellular microvesicles

Verena M. Straub[a], Benjamin Barti[b,1], Sebastian T. Tandar[c,1], A. Floor Stevens[a], Noëlle van Egmond[a], Tom van der Wel[a], Na Zhu[a], Joel Rüegger[a], Cas van der Horst[d], Laura H. Heitman[d,e], Yulong Li[f,g,h], Nephi Stella[i], J. G. Coen van Hasselt[c], István Katona[b,j], and Mario van der Stelt[a,e,2]

Affiliations are included on p. 10.

Edited by Donald Hilgemann, Department of Physiology, The University of Texas Southwestern Medical Center, Dallas, TX; received October 23, 2024; accepted January 16, 2025

While it is known that endocannabinoids (eCB) modulate multiple neuronal functions, the molecular mechanism governing their release and transport remains elusive. Here, we propose an "*on-demand release*" model, wherein the formation of microvesicles, a specific group of extracellular vesicles (EVs) containing the eCB, 2-arachidonoylglycerol (2-AG), is an important step. A coculture model system that combines a reporter cell line expressing the fluorescent eCB sensor, G protein-coupled receptor-based (GRAB)$_{eCB2.0}$, and neuronal cells revealed that neurons release EVs containing 2-AG, but not anandamide, in a stimulus-dependent process regulated by protein kinase C, Diacylglycerol lipase, Adenosinediphosphate (ADP) ribosylation factor 6 (Arf6), and which was sensitive to inhibitors of eCB facilitated diffusion. A vesicle contained approximately 2,000 2-AG molecules. Accordingly, hippocampal eCB-mediated synaptic plasticity was modulated by Arf6 and transport inhibitors. The "*on-demand release*" model, supported by mathematical analysis, offers a cohesive framework for understanding eCB trafficking at the molecular level and suggests that microvesicles carrying signaling lipids in their membrane regulate neuronal functions in parallel to canonical synaptic vesicles.

endocannabinoid | 2-AG | extracellular vesicle | diacylglycerol lipase | cannabinoid 1 receptors

Traditional forms of neurotransmission involve the storage of polar neurotransmitters in synaptic vesicles that fuse with the plasma membrane upon neuronal depolarization, releasing set amounts of neurotransmitters in the synaptic cleft (1). Recently, lipids have emerged as a distinct signaling mechanism to regulate neuronal functions (2). It has been proposed that such lipid messengers, such as the endocannabinoids (eCBs), anandamide and 2-arachidonoylglycerol (2-AG), greatly differ from neurotransmitters as they are not prestored in vesicles due to their lipophilic nature. Instead, they are produced by select stimuli and at a specific time and subcellular site (3, 4). This "on-demand production" model is widely used to explain the regulatory role of eCB on neuronal functions (5–7).

2-AG acts as a retrograde messenger produced by the postsynaptic neuron upon depolarization or activation of metabotropic receptors (8, 9). It traverses the synapse and activates the presynaptic cannabinoid 1 receptors (CB_1R), thereby modulating neurotransmitter release, synaptic plasticity, and neuronal phenotype, as well as complex behaviors related to brain development, learning, memory, appetite, energy balance, pain sensation, and emotional states (10–12). Diacylglycerol lipase-α (DAGLα), a biosynthetic enzyme of 2-AG, plays a crucial role in its "on-demand production" (8, 9). This lipase is highly expressed by neurons and contains a structural motif that binds to Homer proteins, an important component of the molecular scaffold that allows metabotropic glutamate receptor signaling (13). Furthermore, DAGLα activity is regulated by various kinases (14, 15). Genetic deletion or pharmacological inhibition of DAGLα drastically reduces 2-AG levels in the central nervous system (CNS), impairing synaptic plasticity (9), inducing hypophagia (16) and heightening anxiety and fear responses (17, 18).

The termination of 2-AG signaling is hypothesized to occur via its selective uptake from the synaptic cleft by a transport protein, facilitating its diffusion across the plasma membrane (19). To date, the identity of the eCB transport protein remains unknown (20). Once taken up, 2-AG undergoes rapid metabolism by specific enzymes, such as monoacylglycerol lipase (MAGL) and, to a lesser extent, α, β-hydrolase domain-containing protein 6 and 12 (ABHD6 and ABHD12), which together control 2-AG levels in the brain (21). For instance, inhibition of MAGL in the CNS leads to a 10-fold increase in 2-AG levels (22), enhancing depolarization-induced suppression of inhibition (DSI) (23), inducing antinociceptive behavior (24), and exerting anxiolytic effects (25).

Significance

Endocannabinoids (eCB) are lipid neurotransmitters that play a critical role in brain function by activating the cannabinoid CB1 receptor. Unlike classical neurotransmitters, their storage and release mechanisms have remained elusive, leading to major gaps in our understanding of how these signals are regulated. In this study, we developed an experimental system combining genetically encoded fluorescent sensors, electrophysiology, and mathematical modeling to study endocannabinoid signaling with temporal precision. Our findings led us to propose an "on-demand release" model, where microvesicle formation governs endocannabinoid release. This comprehensive model extends the "on-demand production" model and reconciliates the three previously proposed hypotheses for eCB trafficking. The model reshapes our understanding of endocannabinoid signaling and addresses key unanswered questions in the field.

The authors declare no competing interest.

This article is a PNAS Direct Submission.

[1]B.B. and S.T.T. contributed equally to this work.

[2]To whom correspondence may be addressed. Email: m.van.der.stelt@chem.leidenuniv.nl.

This article contains supporting information online at https://www.pnas.org/lookup/suppl/doi:10.1073/pnas.2421717122/-/DCSupplemental.

Published February 20, 2025.

While the current "on-demand production" model captures many features of eCB signaling, it falls short in providing a complete molecular understanding of its release and transport. For example, it fails to explain how hydrophobic lipid messengers like 2-AG (LogP = 6.7) are released from neurons; how the specificity of eCB actions on different cell types is generated; and how they travel from dendrites to CB_1Rs expressed on axon terminals (3, 26). Hence, a deeper understanding of the molecular mechanism governing eCB release and transport remains to be established.

Studying the dynamic changes in eCB levels, however, has been challenging due to the lack of assays capable of tracking endogenously produced eCBs in a spatial, quantitative, and time-resolved manner. Liquid chromatography coupled to mass spectrometry (LC-MS) and the use of radiolabeled eCB have been pivotal techniques for measuring their levels in the context of their transport (27). Although they are powerful tools for specific quantification, they represent snapshots and fail to capture the spatiotemporal nature of eCB signaling. Recently, a genetically encoded fluorescent sensor, $GRAB_{eCB2.0}$, has been developed that allows spatiotemporal resolved imaging of the dynamic changes in eCB levels produced by neurons in culture, acute brain slices, and brain of freely moving animals (28–32). The sensor has, however, not yet been widely used to address the central question of how eCB are released from neuronal cells.

Here, we propose an "on-demand release" model, wherein formation of extracellular microvesicles (EVs) containing 2-AG in their membrane is an important step. Using an eCB transport assay in which neuronal cells are cocultured with a cell line expressing the eCB sensor, $GRAB_{eCB2.0}$, we demonstrate that eCBs are released and transported via the emission of EVs containing 2-AG in a stimulus-dependent process regulated by protein kinase C (PKC), DAGL, and ADP ribosylation factor 6 (Arf6). Each microvesicle contains approximately 2,000 molecules of 2-AG. In addition, we demonstrated that DSI, the prototypical form of eCB-mediated synaptic transmission in acute brain slices, was also modulated by Arf6 and eCB transport inhibitors. Our model, supported by mathematical analysis, provides a comprehensive framework for eCB signaling at the molecular level, potentially explaining why there are different types of endocannabinoids. Our study also suggests an important role for extracellular microvesicles carrying eCB in their membrane in neuronal communication in the CNS, which works in conjunction with classical synaptic vesicles containing polar neurotransmitters.

Results

A $GRAB_{eCB2.0}$-Based Assay to Study eCB Release and Transport. To explore the molecular mechanism underlying paracrine eCB release, we developed a two-culture system using $GRAB_{eCB2.0}$-expressing HEK293T cells alongside Neuro2A cells in microscopy dishes (Fig. 1*A*). Live cell fluorescence confocal microscopy showed that when Neuro2A cells were stimulated with 1 mM of ATP, which activates $P2X_7$ receptors ($P2X_7$Rs) and increases 2-AG levels (33), the $GRAB_{eCB2.0}$ signal on the plasma membrane of nearby HEK293T cells were activated and exhibited fluorescence increase. The fluorescence intensity reached a maximum after 3 min and then gradually declined (Fig. 1*B*). In contrast, no fluorescence response was detected in cocultures with HEK293T cells expressing mutant-$GRAB_{eCB2.0}$, which does not respond to high levels of eCBs (Fig. 1*B*).

Next, we transferred the assay to a 96-well format. Using a fluorescence plate reader, we found that the ratio of 35k HEK293T$_{eCB2.0}$ and 40k Neuro2A cells produced the largest response with minimal background (Fig. 1 *C* and *D*). The ATP-induced $GRAB_{eCB2.0}$ signal was effectively blocked by the CB_1R antagonist, rimonabant (Fig. 1 *F* and *G*), and the $P2X_7$R antagonist, A-740003 (Fig. 1 *H* and *I* and *SI Appendix*, Fig. S2). Treatment with ATP negligible affected the signal of $GRAB_{eCB2.0}$ HEK293T cells cultured alone (Fig. 1 *C* and *D*), while cannabinoid agonist, CP-55,940, added as a positive control, induced a substantial increase in fluorescence (*SI Appendix*, Fig. S1 *C* and *D*).

We also demonstrated the sensor's performance in the optimized transport assay. Direct application of 2-AG, anandamide, and arachidonic acid (AA) showed that 2-AG was the most potent signaling lipid with a pEC_{50} ± SEM of 6.28 ± 0.06, followed by anandamide (pEC_{50} = 6.13 ± 0.08) (Fig. 1*E*). AA did not activate $GRAB_{eCB2.0}$ up to 10 μM, the highest concentration tested. To verify that the ATP-stimulated fluorescence response was mediated by 2-AG, we applied the potent dual DAGLα/β inhibitor, DH376 (1 μM), which completely abolished the fluorescence response of the sensor (Fig. 1 *J* and *K*). As expected, the ABHD6 inhibitor KT182 did not modulate the fluorescent signal (*SI Appendix*, Fig. S3*A*) (33). Together, these findings demonstrate that the two-culture system is suitable to study trans-cellular signaling of endogenously produced 2-AG.

PKC Regulates 2-AG Signaling. First, we leveraged our model system to profile an array of small-molecule inhibitors to uncover regulators of 2-AG synthesis, release, and transport. PKC has been shown to regulate cycling of DAGL between the plasma membrane and EEA1- and Rab5-positive endosomal compartments via a clathrin-independent pathway (34). Inhibiting PKC reduced endocytosis of DAGLα, thereby increasing the pool of this enzyme at the plasma membrane. In line with this result, we found that the PKC inhibitor Sotrastaurin at 1 μM increased $GRAB_{eCB2.0}$ activation to 127 ± 11%, whereas the PKC activator phorbol 12-myristate 13-acetate (PMA) at 100 nM decreased the $GRAB_{eCB2.0}$ sensor response to 54 ± 7.4% (Fig. 2 *A* and *B*). Notably, PKC is also activated by DAG, the substrate of DAGLα (34), suggesting a potential negative feedback mechanism whereby active PKC reduces DAGLα localization at the plasma membrane, thereby decreasing 2-AG signaling.

eCB Transport Inhibitors Reduce 2-AG Signaling. Next, we investigated whether the release and transport of 2-AG was mediated via facilitated diffusion, given that eCBs cross the plasma membrane bidirectionally via an unidentified transporter (35, 36). To this end, we tested three structurally different eCB transport inhibitors: WOBE-437 (27), OMDM-2 (37), and VDM-11 (38), which have been shown to inhibit this process. All three inhibitors significantly reduced ATP-induced $GRAB_{eCB2.0}$ signal in a concentration-dependent manner (Fig. 2 *C*–*H*). WOBE437 was the most potent inhibitor and reduced sensor activation by 50 ± 8% at 10 μM, followed by VDM11 and OMDM-2 with 59 ± 9 and 28 ± 4% reduction, respectively, both at 30 μM.

Fatty acid binding proteins (FABPs), especially FABP5, have also been shown to facilitate intracellular, and possibly extracellular, transport of 2-AG (39, 40) and to modulate eCB-mediated synaptic plasticity (41, 42). In our model system, the FABP5 inhibitor, SBFI-26 (43), partly reduced the ATP-induced sensor signal (Fig. 2 *I* and *J*). Taken together, these results suggest that both the eCB transporter and FABP5 may be involved in the release and transport of 2-AG.

Inhibitors of Extracellular Microvesicles Release Reduce 2-AG Signaling. ATP is known to induce EV release in a $P2X_7$R-dependent manner (44). Since EVs have been reported as carriers of eCB in N9 microglial cells, primary microglia, and midbrain

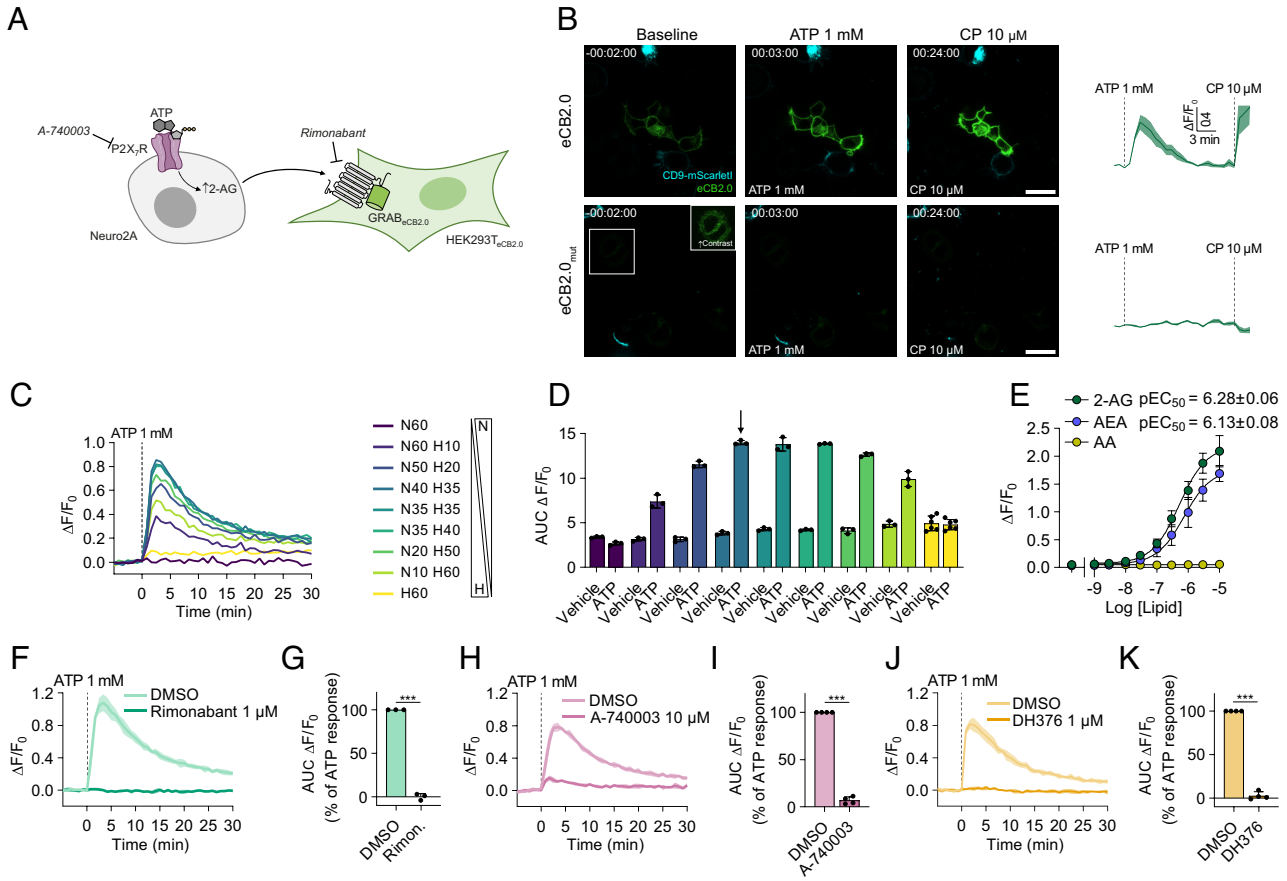

Fig. 1. $GRAB_{eCB2.0}$-based coculture assay to study transcellular 2-AG signaling. (*A*) Schematic representation of the transcellular endocannabinoid transport assay. HEK293T cells expressing $GRAB_{eCB2.0}$ are paired with wild-type Neuro2A cells. Activation of purinergic $P2X_7$ receptors ($P2X_7R$) on Neuro2A cells by exogenous ATP triggers 2-arachidonoyl glycerol (2-AG) production and release. 2-AG released from Neuro2A cells is free to travel and activate $GRAB_{eCB2.0}$ on HEK293T cells. (*B*) Representative confocal images and traces of HEK293T cells transiently expressing $GRAB_{eCB2.0}$ or $GRAB_{eCB2.0mut}$ and Neuro2A cells transiently expressing CD9-mScarletI. Cells were treated with 1 mM ATP. After 20 min, 10 µM CB_1 agonist (−)CP-55,940 was added. Traces show mean $\Delta F/F_0$ ± SEM. n = 3/4 regions of interest for eCB2.0/$eCB2.0_{mut}$. (Scale bars are 20 µm.) (*C*) Traces of different number of $HEK293T_{eCB2.0}$ (H) and Neuro2A (N) cells after treatment with vehicle or 1 mM ATP. (*D*) Area under the curve (AUC) of traces after ATP- or vehicle treatment. The arrow indicates optimal ratio (1:0.875, 40.000 Neuro2A + 35.000 $HEK293T_{eCB2.0}$) with a maximum response to ATP and minimal background signal. Data show mean AUC ± SD. n = 3/6 (H60) wells. (*E*) Dose–response of $GRAB_{eCB2.0}$ activation in the optimized transport assay by 2-AG, anandamide (AEA), and AA. Data are mean ± SD, pEC_{50} values are mean ± SEM [n = 2 (2-AG, AEA)/3 (AA) well plates]. (*F* and *G*) Representative traces (*F*) and AUC of fluorescent changes ($\Delta F/F_0$) (*G*) of cells treated with DMSO or Rimonabant (n = 3 well plates). (*H* and *I*) Same as (*F* and *G*) but cells were treated with DMSO or A-740003 (n = 4 well plates). (*J* and *K*) Same as (*F* and *G*) but cells were treated with DMSO or A-740003 (n = 4 well plates). Traces are shown as mean ± SD (n = 6 wells). AUC was calculated as percentage of vehicle-corrected ATP-response and is shown as mean ± SD. Statistical analysis was performed using a two-tailed *t* test. ***$P < 0.001$.

dopaminergic neurons (45–47), we investigated the role of EVs in the transport of 2-AG. We tested several compounds reported to block different pathways for EV release. Manumycin-A and GW4869, inhibitors of exosome biogenesis via the ESCRT-dependent and ESCRT-independent pathway, respectively (48), did not affect the ATP-induced increase in $GRAB_{eCB2.0}$ signal (*SI Appendix*, Fig. S3 *C–F*). In contrast, SecinH3 and NAV-2729, which primarily target microvesicle release via inhibition of GTPase Arf6 function (47, 49), dose-dependently blocked the ATP-induced increase in $GRAB_{eCB2.0}$ signal (Fig. 2 *K–M*). The response was reduced to 48 ± 3% and 25 ± 2%, respectively (Fig. 2 *L* and *N*). ML-7, an inhibitor of myosin light chain kinase (MLCK), a downstream effector of Arf6 (49), reduced the ATP-induced increase in $GRAB_{eCB2.0}$ signal to 57 ± 6% (Fig. 2 *O* and *P*) (50). Of note, none of the agents significantly affected $GRAB_{eCB2.0}$ signal in HEK293T cells stimulated with CP-55,940, nor was any cytotoxicity observed (*SI Appendix*, Fig. S4 *A–J*). Together, these data suggested that microvesicle release, but not exosome release, which is controlled by Arf6 and MLCK, is involved in ATP-stimulated 2-AG release and transport.

Finally, we tested whether 2-AG production and release can be induced via activation of the metabotropic bradykinin receptor B_2 with bradykinin (BK) (51–53) and through a similar mechanism as activation of the ionotropic $P2X_7R$. Indeed, BK treatment of Neuro2a cells led to an increase in $GRAB_{eCB2.0}$ signal on HEK293T cells, which was blocked by DH376, WOBE437, and SecinH3 (*SI Appendix*, Fig. S5), suggesting a common mechanism for metabotropic and ionotropic-induced 2-AG release and transport.

Microvesicles Carry 2-AG. To obtain an independent line of evidence supporting 2-AG release via extracellular microvesicles, we isolated and characterized EVs from Neuro2A cell culture supernatant using previously reported methods (Fig. 3*A*). ATP increased the EV release by twofold as assessed by EV marker protein CD9 detected by western blot, which could be partly blocked by the $P2X_7R$ antagonist A-740003 (Fig. 3 *B* and *C*). Nanoparticle tracking analysis (NTA) confirmed the increase in number of EVs following addition of ATP (Fig. 3 *D* and *E*). The EVs were of medium to large size ranging from 100 to 600 nm (Fig. 3*D*) with a mean size of 296 ± 19.0 nm (Fig. 3*G*). Stimulation with ATP did not alter the size distribution of isolated vesicles (Fig. 3 *D*, *F*, and *G*). Following ATP stimulation, cells released 7.2 ± 2.4 10^8 particles, which equates to around 65 ± 25 vesicles released per cell.

We further characterized the EVs by LC-MS/MS-based proteomics, which led to the identification of 1,160 proteins more

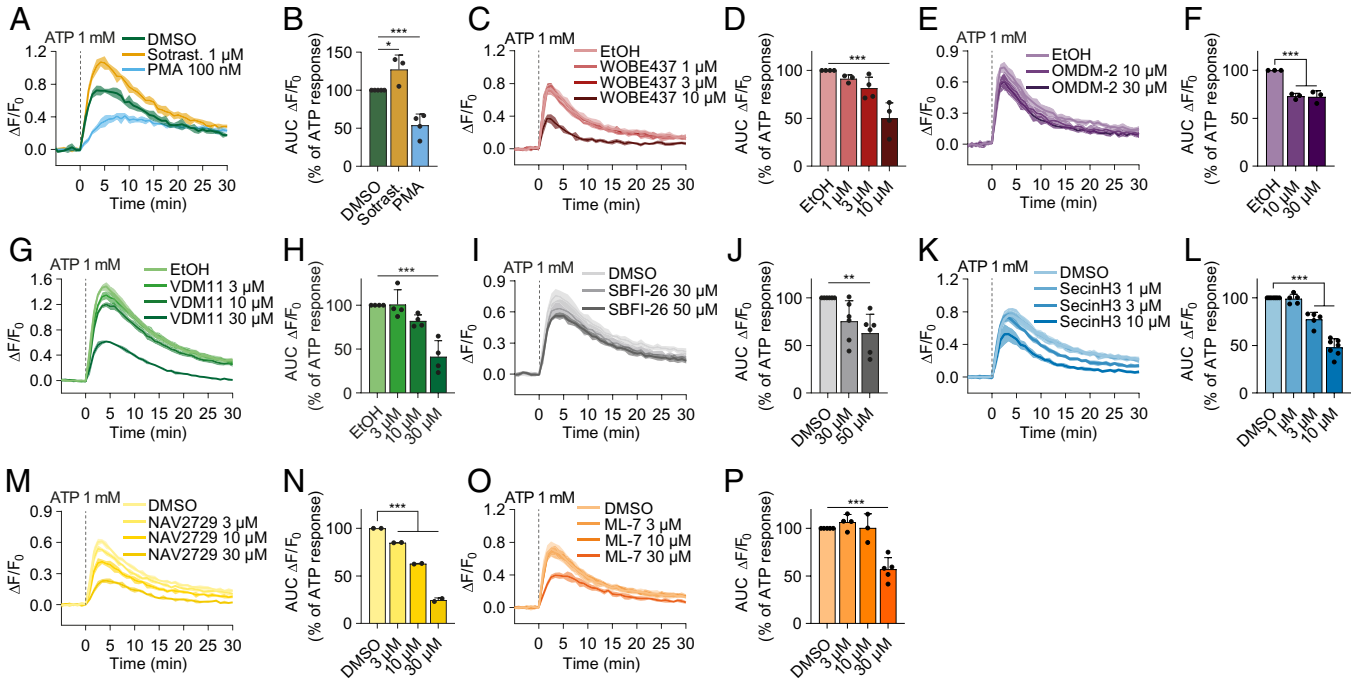

Fig. 2. Pharmacological screening reveals regulators of 2-AG release and transport. (*A* and *B*) Representative traces (*A*) and AUC of fluorescent changes ($\Delta F/F_0$) (*B*) of cells treated with DMSO, Sotrastaurin or PMA (n = 5/3/4 DMSO/Sotrastaurin/PMA). (*C* and *D*) Same as (*A* and *B*) but cells were treated with EtOH or WOBE437 (n = 4/3/4/4 EtOH/3 µM/10 µM/30 µM). (*E* and *F*) Same as (*A* and *B*) but cells were treated with EtOH or OMDM-2 (n = 3). (*G* and *H*) Same as (A and B) but cells were treated with EtOH or VDM11 (n = 4). (*I* and *J*) Same as (*A* and *B*) but cells were treated with DMSO or SBFI-26 (n = 6). (*K* and *L*) Same as (*A* and *B*) but cells were treated with DMSO or SecinH3 (n = 7/5/5/7 DMSO/1 µM/3 µM/10 µM). (*M* and *N*) Same as (*A* and *B*) but cells were treated with DMSO or NAV2729 (n = 2). (*O* and *P*) Same as (*A* and *B*) but cells were treated with DMSO or ML-7 (n = 5/4/3/5 DMSO/3 µM/10 µM/30 µM.). AUC was calculated as percentage of vehicle-corrected ATP-response. Data are shown as mean ± SD. Statistical analysis was performed using one-way ANOVA with Tukey's correction for multiple comparisons. n for traces is individual wells and n for AUC is independent well plates. **P* < 0.05, ***P* < 0.01, ****P* < 0.001.

than 10-fold enriched in EV preparations compared to Neuro2A cell lysate. Proteins related to the extracellular space/region, plasma membrane, and extracellular exosome were overrepresented by cellular component gene ontology analysis (Fig. 3*H*). Multiple EV marker proteins were detected, including CD9, CD63, CD81, CD82, ADAM10, SNARE proteins, syntenin-1, EHD4, and Annexin-A5 (Fig. 3 *I* and *J*). In turn, marker proteins for several cellular organelles (HIST1H1A, CYC1, Calnexin, TOMM20, and GM130) were significantly reduced in EVs compared to Neuro2A cell lysates, validating the identity and purity of the isolated EVs (Fig. 3*J*). Of note, ARF6, FABP5, and SCP-2 were also found in the EV fractions. Further analysis of molecular functions and biological pathways associated with proteins enriched in EVs revealed that integrin binding, receptor binding, heparin binding, and collagen binding were significantly overrepresented in EVs compared to the cell lysate. Among the biological pathways, cell adhesion and cell–matrix adhesion were two of the three most enriched (*SI Appendix*, Fig. S6). Taken together, this suggests that these vesicles contain several components of the 2-AG release and transport machinery and may be targeted to the surface of specific recipient cells.

Next, we probed whether eCB and related lipids were contained in the EVs using LC-MS/MS-based targeted lipidomics. We measured a lipid panel of 26 signaling lipids, composed of 2-AG, anandamide, and their analogues as well as free fatty acids. Out of the 26 lipid species, 17 could be identified in Neuro2A EVs above the limit of detection (LoD) of our LC-MS/MS method (*SI Appendix*, Fig. S7), including 2-AG and AA, but not anandamide (LoD = 0.01 nM). In addition to 2-AG, monoacylglycerols 2-oleoylglycerol (2-OG) and 2-lineoyl glycerol (2-LG) were identified. Of the free fatty acids, oleic acid, linoleic acid, palmitic acid, stearic acid, eicosatrienoic acid (ETA), and dihomo-γ-linolenic acid (DGLA) were found in EVs. Additionally, *N*-stearoylethanolamine, *N*-palmitoylethanolamine, *N*-oleoylethanolamine, *N*-linoleoyl ethanolamine, and *N*-pentadecanoyl ethanolamine were detected in EVs.

Remarkably, 2-AG and AA levels were significantly increased to 139 ± 7% and 153 ± 13%, respectively, in the EV preparations following ATP stimulation (Fig. 4*A*). Importantly, 2-AG was not detected in protein-containing fractions 9 + 10 and cellular levels of all lipids remained unchanged (Fig. 4*B* and *SI Appendix*, Fig. S8). ETA, DGLA, 2-OG, and 2-LG levels in EVs were slightly increased, but these changes did not reach statistical significance (*SI Appendix*, Fig. S7). In contrast to the studies of Gabrielli et al. (45) and Lombardi et al. (46), anandamide in Neuro2A EVs was below the LoD, which could be due to differences in the EV isolation protocol or, more likely, due to the different cell types studied.

Taking the average particle count of EVs released by ATP-stimulated cells as determined by NTA ($7.2 \pm 2.4 \times 10^8$) and the average absolute 2-AG levels (2,507 ± 706 fmol), each vesicle contained an estimated number of 2,000 2-AG molecules. If all isolated vesicles contain 2-AG to the same extent, the average number of 2-AG molecules per vesicle with or without ATP stimulus remained constant. This would suggest that the increased number of vesicles released by ATP is sufficient to explain the $GRAB_{eCB2.0}$ response. However, 2-AG and AA were the only lipids significantly increased in the total pool, therefore it is conceivable that ATP triggers the release of specific EV subsets that are enriched in 2-AG and AA levels. In summary, we show that ATP induces the release of extracellular microvesicles from Neuro2A cells that contain 2-AG, but not anandamide.

DAGL and Arf6 Regulate Release of 2-AG in Microvesicles. Subsequently, we investigated whether the ATP-induced increase in 2-AG in EVs depends on DAGL activity. Incubation of Neuro2A cells with 1 µM of DH376 prior to ATP-stimulation and EV isolation did not alter the number or size distribution

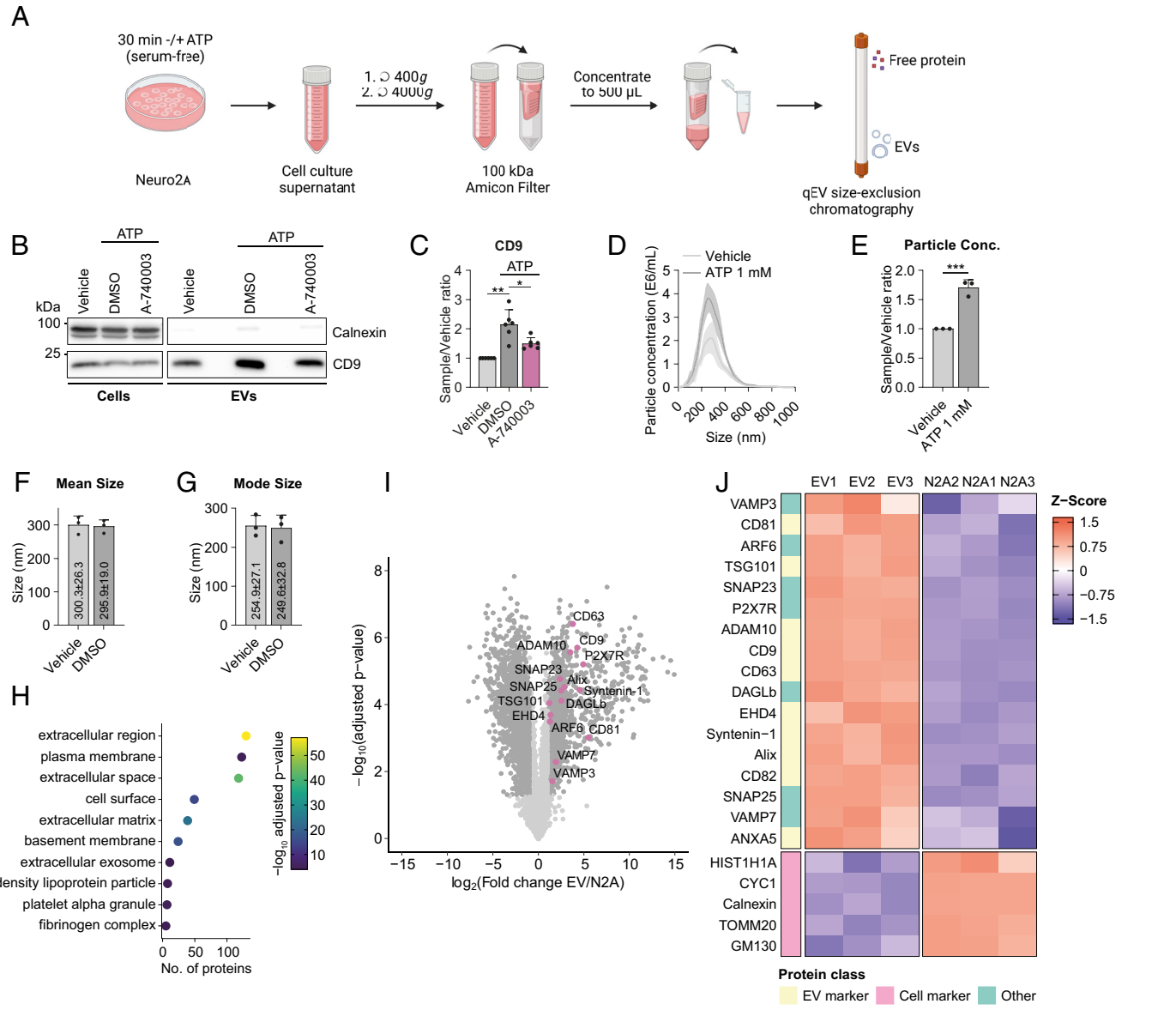

Fig. 3. ATP stimulates $P2X_7R$-dependent microvesicle release from Neuro2A cells. (*A*) Schematic representation of EV isolation process. Release of EVs is stimulated by 1 mM ATP for 30 min under serum-free conditions. Cell culture supernatant is collected and cleared from cells and cell debris. Supernatant is concentrated to 500 µL using 100 kDa centrifugal filters. EVs are separated from free protein by size-exclusion chromatography (SEC) using Izon qEV 30 nm columns. Created with biorender.com. (*B*) Representative western blot of cell lysates and EVs following treatment with DMSO or 10 µM A-740003 (20 min, 37 °C) and stimulation with 1 mM ATP or MQ (30 min, 37 °C). (*C*) Quantification of CD9 signal intensity. Fold change is calculated relative to the respective vehicle control. Data are shown as mean ± SD (n = 6 independent biological experiments). Statistical analysis was performed using matched one-way ANOVA with Tukey's correction for multiple comparisons. (*D*) Representative size distribution of EVs determined by nanoparticle tracking analysis. Data is mean ± SD (n = 3 videos). (*E–G*) Fold change of particle concentration (*E*), mode size (*F*), and mean size (*G*) of EVs as determined by NTA. Data are shown as mean ± SD (n = 3 independent biological experiments). Statistical analysis in (*E*) was performed using a two-tailed *t* test. (*H*) Gene ontology enrichment analysis for cellular compartment of proteins enriched >10-fold in EVs compared to Neuro2A cell lysate as determined by LC-MS/MS-based proteomics. (*I*) 5,181 proteins were identified in EVs. Fold change of protein intensity in EVs compared to Neuro2A cell lysate is shown. Proteins of interest are highlighted. (*J*) Scaled protein abundance of selected proteins in EVs and Neuro2A cells (N2A). EV1-3 and N2A1-3 represent biological replicates. $*P < 0.05$, $**P < 0.01$, $***P < 0.001$.

of released EVs (Fig. 4 *C–E*), but the increase of 2-AG and AA content in EVs was blocked (Fig. 4*F* and *SI Appendix*, Fig. S7). This suggests that 2-AG produced by DAGL is loaded into EVs and that its incorporation can be uncoupled from the release of EVs. In turn, we next asked whether a reduction in EV release influences the 2-AG content detected in EVs. To this end, we interfered with ATP-stimulated EV release by SecinH3-mediated inhibition of Arf6 activity. Western blot analysis showed a 43 ± 19% reduction in CD9 levels in line with the particle analysis (Fig. 4 *I* and *J*). 2-AG levels in cells were not changed following SecinH3 treatment (Fig. 4*L*). In EV preparations, however, SecinH3 blocked the increased levels of 2-AG following ATP stimulation (Fig. 4*K*). This showed that while SecinH3 does not influence 2-AG biosynthesis itself (because cellular 2-AG levels remained unchanged), it reduced the number of EVs and thereby the total content of 2-AG in the extracellular space. Of note, the 2-AG level in the EVs was only 0.25% of the total cellular pool, which is in line with previous reports (12). The small extracellular pool compared to the bulk 2-AG cellular levels, which were both dependent on DAGL biosynthesis, indicate that 2-AG remains in the cell and does not spontaneously diffuse into the aqueous extracellular environment. Taken together, this suggests that 2-AG is specifically sorted into extracellular microvesicles in an Arf6-dependent mechanism and released upon an ATP stimulus.

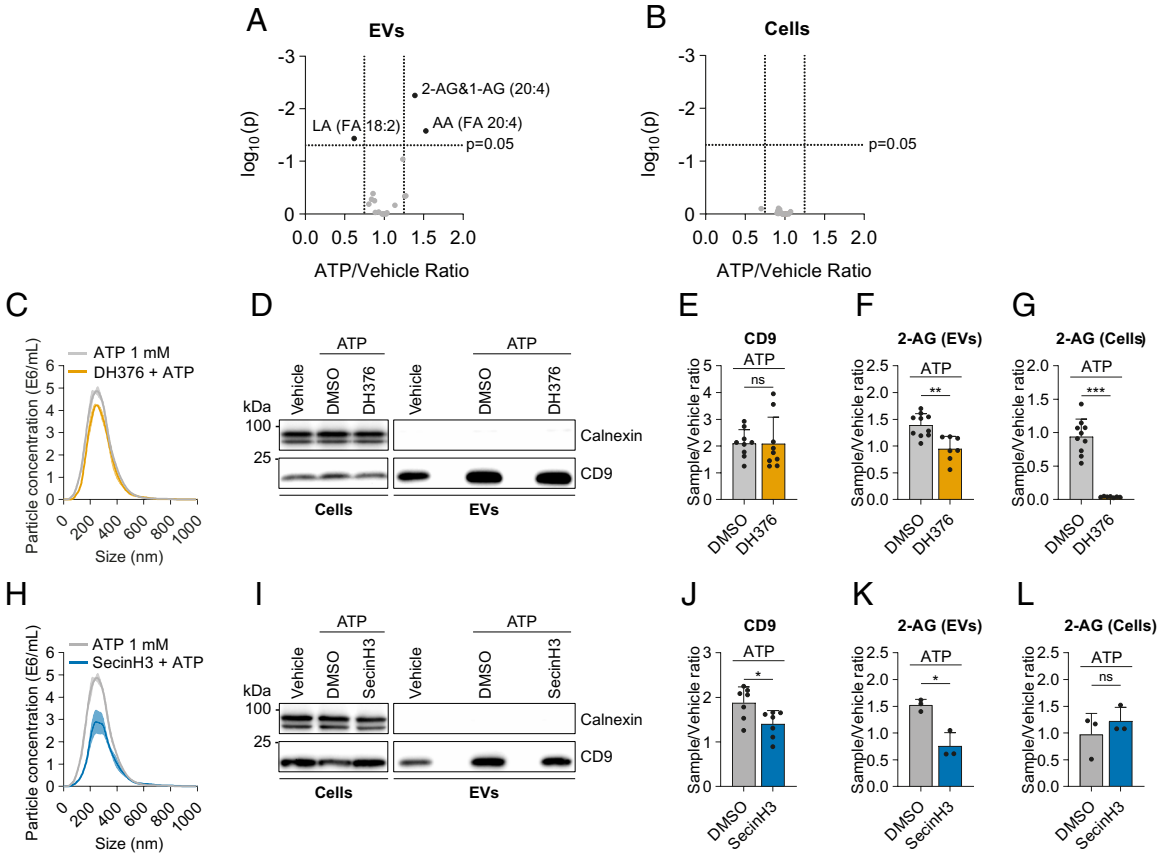

Fig. 4. 2-AG is specifically sorted into microvesicles in a DAGL- and Arf6-dependent process. (*A* and *B*) Fold-enrichment (ATP/Vehicle) of lipids in EVs (*A*) or cells (*B*) following vehicle (MQ) or ATP-treatment for 30 min at 37 °C. (*C*) Size distribution of EVs determined by nanoparticle tracking analysis (NTA) (n = 3 videos). (*D*) Representative western blot and (*E*) quantification of CD9 signal intensity in EVs (n = 9). (*F* and *G*) 2-AG levels in EVs (*F*) and cells (*G*) relative to vehicle-treated control (n = 10/7 DMSO/DH376). (*H*) Size distribution of EVs determined by nanoparticle tracking analysis (NTA) (n = 3 videos). (*I*) Representative western blot and (*J*) quantification of CD9 signal intensity in EVs (n = 7). (*K* and *L*) 2-AG levels in EVs (*K*) and cells (*L*) relative to vehicle-treated control (n = 3). Cells were treated with 1 μM DH376 (*C*–*G*) or 10 μM SecinH3 (*H*–*L*) for 20 min prior to vehicle (MQ) or ATP-treatment for 30 min at 37 °C, followed by EV isolation. Data are shown as mean ± SD. n is individual biological replicates/EV isolations. Statistical testing was performed using one-way ANOVA with Tukey's correction for multiple comparisons. **P* < 0.05, ***P* < 0.01, ****P* < 0.001, ns not significant *P* > 0.05.

DSI Involves Arf6. Next, we aimed to translate our key findings to an acute hippocampal slice model, where the molecular and cellular organization of the brain circuit remains largely intact, to investigate whether Arf6 plays a role in 2-AG-mediated synaptic plasticity. First, we confirmed that primary hippocampal neurons produce 2-AG in a stimulus-dependent manner via DAGL and Arf6, using our transport assay (*SI Appendix*, Fig. S9). Next, we examined whether DSI, a prototypical form of eCB-mediated synaptic plasticity, is controlled by Arf6 and eCB transport inhibitors. To test this, we conducted paired-patch clamp recordings between CB_1 receptor-positive basket cells and pyramidal cells (PC) in acute hippocampal slices, infusing Arf6 or eCB transport inhibitors into the postsynaptic neuron via the patch pipette (Fig. 5*A*). We found that the synaptic charge transferred during inhibitory postsynaptic currents (IPSCs), a strong readout for DSI efficacy, was affected by SecinH3, NAV2729, and WOBE437 (Fig. 5 *B*–*F*). Differences were already apparent shortly after the start of the experiment and became even more pronounced after more than 20 min of recording (Fig. 5 *C*–*F*). Importantly, the synaptic charge remained unaffected during baseline synaptic transmission when DSI was not induced (Fig. 5*B*). In contrast, the inhibitors reduced DSI (Fig. 5 *D*–*F*), indicating a specific alteration of phasic 2-AG-mediated signaling without affecting baseline synaptic activity. Notably, the initial amplitude of DSI was unaffected by the inhibitors, suggesting a delayed onset of the effects of the intracellularly applied inhibitors and an effect on persistence of DSI rather than initial induction. Considering the 20 min intracellular drug infusion of the postsynaptic cell, the delayed onset is unlikely attributed to technical factors such as slow diffusion. The faster decay of DSI induced by the inhibitors suggests that less 2-AG is available in the presynaptic neuron to activate the CB1 receptor, indicating that 2-AG uptake and metabolism is the rate-determining step in DSI. This finding aligns with previous studies (23, 54). Moreover, prior incubation of slices in ACSF solution containing the inhibitors did not reveal differences in baseline synaptic transmission properties and DSI duration in pairs investigated (*SI Appendix*, Fig. S10), which argues for a specific role of inhibitors applied in the postsynaptic intracellular solution. Together, these results suggest that phasic 2-AG signaling in hippocampal slices involves Arf6 and the unidentified endocannabinoid membrane transporter. While our electrophysiological data closely align with key findings from our transport assay using cultured cells, we cannot exclude the possibility that the role of Arf6 in DSI extends beyond EV release due to its involvement in other cellular mechanisms (55), or that additional mechanisms may also be involved.

Formation of Extracellular Microvesicles Containing 2-AG is the Rate-Limiting Step in Neuro2A Cells. Finally, to determine the rate-limiting step in 2-AG release in Neuro2A cells, we developed a mathematical model of reporter cell activation (Fig. 6*A* and *SI Appendix*). The model considers 2-AG production, metabolism, and distribution between a main Neuro2A cellular 2-AG pool (m_{cell}) and an EV pool located in the plasma membrane (m_{EV}). The

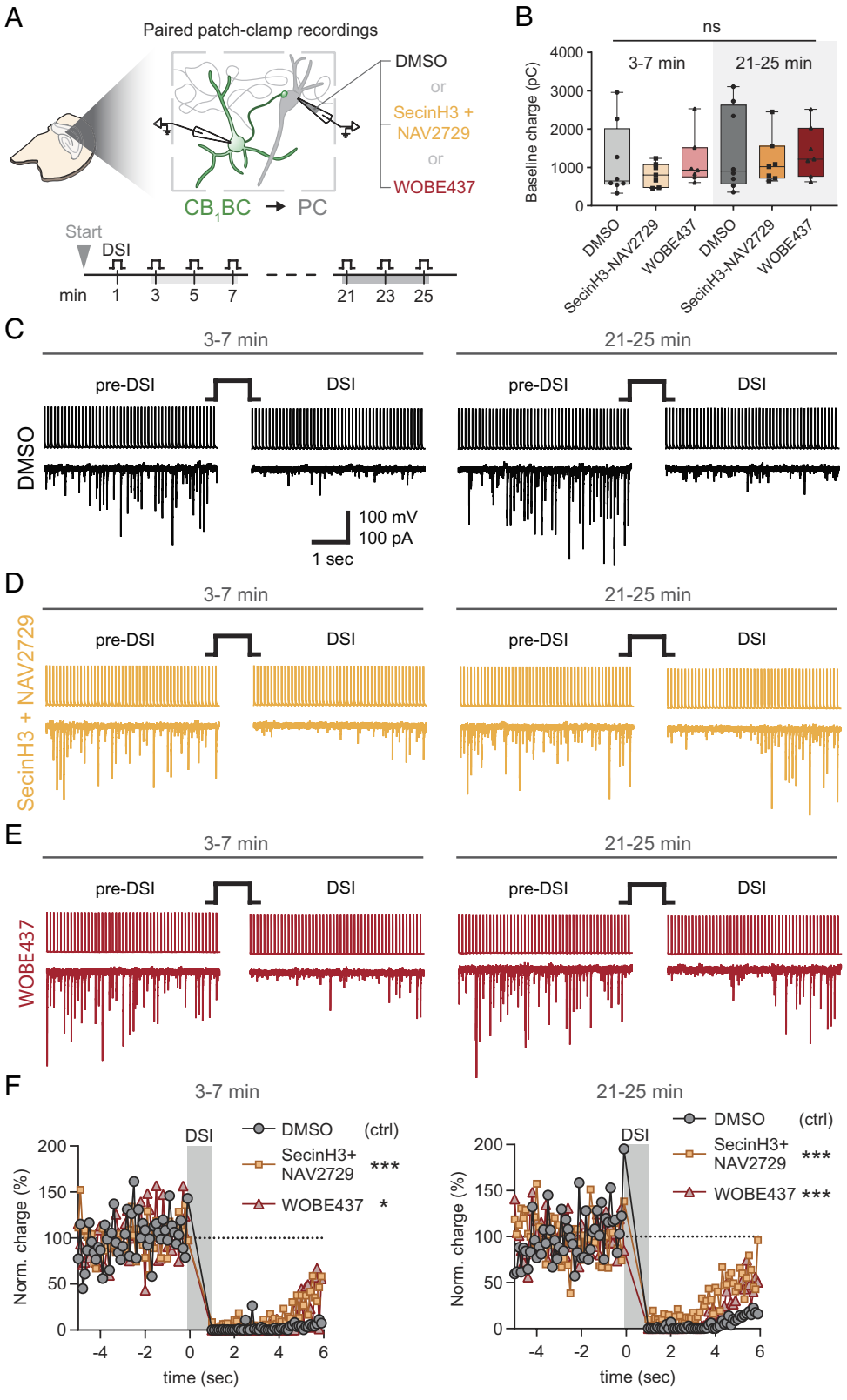

Fig. 5. Inhibition Arf6 and facilitated diffusion affects 2-AG-dependent phasic endocannabinoid signaling ex vivo. (*A*) Schematic illustration of experimental design. Paired patch-clamp recordings were conducted in acute hippocampal slices between CB_1-positive basket cells (CB_1BC) and PC. The intracellular solution for the postsynaptic cell contained either vehicle DMSO, SecinH3 and NAV2729 or WOBE437 in the pipette. DSI was induced with 1 s depolarization of the postsynaptic cell in every 2 min after the start of the experiment. The timeline of the experiment represents analyzed time windows. (*B*) Summary graphs of baseline synaptic charge between pairs. (*C*) Representative traces of presynaptic action potential evoked (*Top* traces) IPSCs (*Bottom* traces) before and after DSI induction at 3 to 7 min and 21 to 25 min time windows. Postsynaptic intracellular solution contained vehicle 0.5% DMSO. (*D*) Same as (*C*), but postsynaptic intracellular solution contained SecinH3 (10 μM) and NAV2729 (30 μM). (*E*) Same as (*C* and *D*), but postsynaptic intracellular solution contained WOBE437 (10 μM). (*F*) Summary plots of normalized charge values before and after DSI induction at 3 to 7 min and 21 to 25 min time windows. Data show median ± IQR with individual datapoints (*B*) or mean (*F*). Statistical significance was determined by the Kruskal–Wallis test with Dunn's multiple comparisons (*B*) or repeated measures one-way ANOVA with Dunnett's multiple comparisons (*F*). *P < 0.05, ***P < 0.001, ns not significant P > 0.05. N = 7 animals/group n = 8/7/7 individual pairs in groups DMSO/SecinH3 and NAV2729/WOBE437, respectively.

EV pool represents 2-AG sorting into the membrane of forming microvesicles. An ATP stimulus releases EVs containing 2-AG from the plasma membrane into the extracellular space. A fraction of the extracellular 2-AG is absorbed by the adjacent cells in which 2-AG is distributed and metabolized. The 2-AG concentration in the reporter cell determines the observed fluorescent signal strength generated by the $GRAB_{eCB2.0}$ sensor.

The model was fitted to describe and quantify the characteristics of the experimentally observed signal dynamics of ATP-stimulated Neuro2A cells (Fig. 6*B* and *SI Appendix*). Notably, the inclusion of m_{EV} in Neuro2A cells in the model was necessary to capture the dynamics of signal peak formation observed at approximately 220 s after the ATP stimulus. In contrast, an alternative model structure which takes only 2-AG production into account, and not the 2-AG sorting into the membrane of forming microvesicles, could not replicate the formation of the signal peak (Fig. 6*B* and *SI Appendix*), suggesting the presence of preformed microvesicles in Neuro2A cell before the ATP stimulus.

Using the model, we estimated that 59% of 2-AG molecules in the extracellular space was originally present in the membrane of preformed microvesicles and released in 38 vesicles per Neuro2A cell during the initial burst. The remaining 2-AG was released in a distinctly lower rate of one vesicle every approximately 67 s after the initial signal burst. The fill rate constant k_{fill} of the microvesicle pool was 5.7×10^{-7} s^{-1}, which is significantly smaller than the 2-AG production rate constant k_{prod} (6.7×10^{-3} s^{-1}). Consequently, the model predicts that it takes substantial time (>60 min) to completely regenerate the m_{EV} pool with 2-AG upon depletion. Of note, the absorption rate constant k_{abs} (1.3×10^{-7} s^{-1}) was approximately fivefold lower than k_{fill}. In summary, the model suggested that the formation of microvesicles loaded with 2-AG is the rate-limiting step in eCB release from Neuro2A cells rather than 2-AG production, while the uptake of 2-AG by the reporter cell is the overall rate-determining step in $GRAB_{eCB2.0}$ sensor activation.

Discussion

There are three current hypotheses to explain cellular eCB trafficking: a) (intra)cellular transport via lipid carrier proteins (41, 42); b) transport and release via extracellular vesicles, (45–47); and c) release and reuptake via unidentified membrane transporters (27). Yet, the molecular mechanism how eCBs are released from neuronal cells is poorly understood (11). To address this important

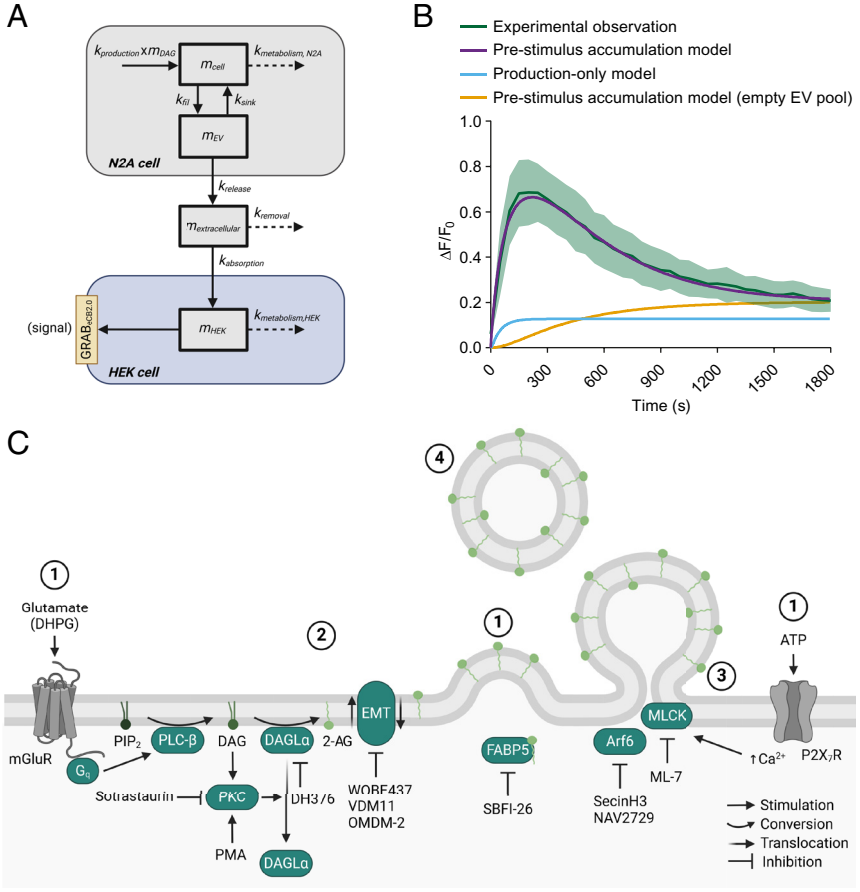

Fig. 6. Model for on-demand 2-AG release in extracellular microvesicles. (*A*) Schematic of the mathematical compartmental model to approximate $GRAB_{eCB2.0}$ activation in the endocannabinoid transport assay. (*B*) Model fitting shows that the implementation of a preformed EV pool is important to describe the formation of the observed signal peak. A model that only takes 2-AG production into account was unable to capture the dynamics of the signal peak. (*C*) Scheme on the on-demand release model (1) Stimulation of the cell leads to lipid shuffling and cytoskeleton rearrangements, resulting in the formation of a budding plasma membrane microvesicle. (2) 2-AG is loaded into forming microvesicles. This process is regulated by production of 2-AG by DAGLα; PKC-dependent endocytosis of DAGLα; translocation of 2-AG within the lipid bilayer by an unidentified endocannabinoid transporter; and intracellular endocannabinoid transport proteins. (3) Release of budding vesicles through membrane fission is controlled by Arf6- and MLCK-activity. (4) 2-AG containing extracellular vesicles released into the extracellular space mediate cell-to-cell communication and may be taken up by various cell types to terminate endocannabinoid signaling. 2-AG: 2-arachidonoylglycerol, Arf6: ADP-ribosylation factor 6, ATP: Adenosine triphosphate, DAG: Diacyl glycerol, DAGLα: DAG lipase α, DHPG: (*S*)-3,5-dihydroxyphenylglycine, EMT: Endocannabinoid membrane transporter, FABP5: Fatty-acid binding protein 5, G_q: Heterotrimeric G protein alpha subunit q, mGluR: Metabotropic glutamate receptor, MLCK: Myosin light chain kinase, $P2X_7R$: $P2X_7$ receptor, PIP_2: Phosphatidylinositol-4,5-bisphosphate, PKC: Protein kinase C, PLC-β: Phospholipase C-β, PMA: Phorbol 12-myristate 13-acetate. Created with biorender.com.

subject, we developed an eCB reporter cell line by introducing the eCB sensor $GRAB_{eCB2.0}$ into HEK293T cells (28), and combined it in a 96-well plate format with mouse neuroblastoma Neuro2A cells, commonly used for studying eCB signaling (56). Leveraging this model system, we demonstrated that activated neuronal cells release microvesicles containing 2-AG in a process regulated by PKC, DAGL, Arf6, and which is sensitive toward inhibitors of eCB facilitated diffusion. Key findings were replicated in primary hippocampal neurons and acute hippocampal slice preparations. We demonstrated that DSI, a prototypical form of eCB-mediated synaptic transmission, was also modulated by Arf6 and eCB transport inhibitors. Based on the literature (vide infra), our experimental findings, and mathematical analysis, we propose an "on-demand release" model, where the formation and stimulus-dependent release of extracellular microvesicles containing 2-AG constitutes an important step (Fig. 6*C*). This model involves the following four steps:

1. Activation of neurons leads to membrane budding. The activation of neurons induces membrane budding. This process is triggered by stimuli like synaptic activity (44, 57), metabotropic and ionotropic receptor stimulation, leading to calcium-dependent rearrangements of the cytoskeleton (57) and membrane lipids (58–60), culminating in the protrusion of the plasma membrane (60–62).
2. Sorting of 2-AG into outward budding plasma membrane: 2-AG is sorted into the outward budding plasma membrane, which relies on its biosynthesis by DAGLα at the plasma membrane (29, 63). DAGLα activity and its subcellular localization is dynamically regulated via kinases like PKA, PKC, and CaMKII (14, 15) and interactions with Homer-proteins situated in neuronal subdomains close to the metabotropic glutamate receptor and rich in the EV marker Flot-1 (13). The transportation of 2-AG into outward budding plasma membrane may involve eCB transporters, which could act as lipid scramblases facilitating 2-AG diffusion between bilayer leaflets (64), although further research, including the identification of the target proteins of the transporter inhibitors, is needed to fully understand this process (65, 66).

   Lipid carrier proteins like FABP5, HSP70, and SCP2 may play an additional role in transporting 2-AG from other organelles, as well as lipid droplets, to the membrane of the forming microvesicles (41, 42). The cargo-loading of microvesicles also involves SNARE proteins (62, 67, 68), with postsynaptic synucleins and synaptobrevin (VAMP2) being necessary for the release of eCB (31). Thus, the sorting of 2-AG into the membrane of the vesicles is governed by multiple pathways, likely influenced by the cell type, subcellular origin of 2-AG and the specific subset of vesicles released.
3. Membrane fission leads to microvesicle release: The connection between newly formed vesicle and the cell membrane is eventually severed through membrane fission. Arf6 plays a crucial role by recruiting MLCK to phosphorylate MLC at the vesicle neck, leading to actin cytoskeleton remodeling and EV release (49, 60, 69). Notably, we found a delayed onset of action of the Arf6 and transport inhibitors in the modulation of hippocampal synaptic transmission. This suggests that preexisting microvesicles, i.e., plasma membrane protrusions associated with MLCK, are waiting to be released upon a physiological stimulus. We term these protrusions "primed microvesicles." Since primed microvesicles are still part of the plasma membrane, (stimulus-induced) 2-AG biosynthesis by DAGL and the fast lateral diffusion of 2-AG enables its equilibrium in the primed vesicles. Inhibition of DAGL depletes 2-AG from the plasma membrane and, therefore also from the primed microvesicles. Once the primed vesicles are released on demand, the subsequent time-dependent formation of new microvesicles and their loading with 2-AG become dependent on Arf6 and the putative eCB transporter. This mechanism may explain the distinction between the dynamics of DAGL inhibition and Arf6 inhibition on DSI.
4. Removal of extracellular microvesicles limits 2-AG signaling: EVs containing eCBs like 2-AG play a crucial role in cell-to-cell communication in the CNS (45–47, 70). Signaling lipids can be efficiently transferred from microvesicles to plasma membranes upon collision or membrane fusion rather than via phagocytosis or endocytosis, which is a slower process (71, 72), but future studies, such as real-time imaging of EV interactions with CB_1R expressing cells or the use of tagged 2-AG molecules, could help to clarify this mechanism.

The activation of CB_1R depends on several factors: the number of vesicles interacting with the target cell, the concentration of 2-AG within the vesicle, and the 2-AG diffusion gradient, which is influenced by the distribution of 2-AG and the activity of 2-AG metabolizing enzymes such as MAGL, ABHD6, ABHD12, and MGAT in the CB_1R-expressing target cell (65). Additionally, astrocytes and microglia may absorb EVs from the synaptic cleft, potentially limiting 2-AG signaling and contributing to retrograde endocannabinoid signaling at the synapse (73, 74). Notably, the uptake and metabolism of 2-AG is the overall rate-limiting step in CB_1R signaling and DSI (23, 54).

Implications of the On-Demand Release Model. The release of microvesicles containing 2-AG from cells may reflect the metabolic state of a cellular network, as 2-AG is part of the futile lipid cycle characterized by a high metabolic flux, where its biosynthesis and metabolism are in equilibrium (75). Release of 2-AG-containing vesicles enables neighboring cells expressing CB_1R to sense the network's metabolic state. In addition, an activity-dependent rapid increase in 2-AG production or microvesicle release, such as due to neuronal activity would then serve to control network activity through CB_1R-mediated inhibition of neurotransmitter release.

Anandamide was not detected in microvesicles derived from the plasma membrane in our experimental setting but was previously identified in exosomes from microglia (45). The biosynthetic machinery of anandamide is primarily found on presynaptic, intracellular membranes (76), and anandamide can function as an intracellular messenger, thereby acting in an autocrine-like manner (77). This may suggest that the intracellular anandamide concentration reflects activation of presynaptic metabolic processes (76). Since the signaling pool of 2-AG was only 0.25% of its total cellular pool, this indicates that anandamide and 2-AG concentrations available to activate CB_1R are in the same order of magnitude. We propose, therefore, that the CB_1R expressed on presynaptic terminals or astrocytes can act as a sensor integrating the metabolic state from both post- and presynaptic sites by detecting the para- and autocrine signaling of eCBs. Intriguingly, this may also explain why there are two different types of eCB. Anandamide could represent the metabolic state of presynaptic sites, whereas 2-AG reflects postsynaptic metabolic processes in a cellular network.

EVs contain (glyco)proteins, such as lectins and integrins, which may facilitate the targeting of EVs to specific cell types or sites expressing cognate receptors. Interestingly, this could potentially explain the cell-type specificity of eCB signaling (26, 78). Moreover, EVs may extend beyond the synapse, activating CB_1R at distant sites [e.g., on perisomatic GABAergic terminals (3, 79)]

or even entering the general circulation, allowing eCB to travel in the body and convey information to cells in other organs about the metabolic state of their site of origin.

One of the limitations of our study is that the molecular mechanism of microvesicle formation and release is poorly understood, thereby complicating the interpretation of the data. Our two-culture model may be leveraged to perform chemical genetic screens, such as CRISPRi, to identify the proteins involved in these processes. Furthermore, we cannot exclude that different cells may use additional mechanisms for eCB release. Our study was performed using in vitro and ex vivo models, therefore they do not confirm whether the model is operational in an in vivo setting. Establishing the relevance of EV-mediated 2-AG transport in vivo would require innovative approaches. For instance, the use of animal models with genetically encoded markers and biosensors for EV-release and 2-AG signaling, combined with in vivo imaging and targeted inhibition of EV release pathways, could shed light on whether this mechanism plays a role in vivo. Additionally, leveraging in vivo electrophysiology in conjunction with pharmacological manipulations of EV release may help link these findings to physiological processes.

To conclude, the development of a two-culture model featuring a genetically encoded fluorescent sensor capable of detecting eCB levels, enabled the time-resolved study of eCB production, release, and trafficking between cells. This led us to propose a "on-demand release" model, supported by mathematical analysis and electrophysiological studies, wherein the formation and stimulus-dependent release of extracellular microvesicles containing 2-AG in their membrane is an important step. This model extends the previously proposed "on demand production" model and reconciliates the three previously proposed hypotheses for eCB trafficking. It provides a cohesive and quantitative framework for understanding of eCB signaling at the molecular level that can be tested by future experimental studies. Given that CB_1R is one of the most abundant G protein–coupled receptor in the brain and eCBs are found in every brain region constituting diverse neuronal circuitries, our study suggests an important role of extracellular microvesicles carrying hydrophobic signaling lipids as a mechanism to regulate neurotransmission in the nervous system in addition to classical synaptic vesicles containing polar neurotransmitters.

Materials and Methods

An extended section is provided in *SI Appendix, Supporting Experimental Procedures*. Animal experiments conducted in the United States were approved by the Institutional Animal Care and Use Committee of Indiana University and conform to the NIH Guidelines on the Care and Use of Animals. Animal procedures at Leiden University were approved by the Ethics Committee for Animal Experiments and the Animal Welfare Body of Leiden University (AVD10600202215851; 15851,1-193) and were performed in accordance with the guidelines of the Dutch government and the European Directive 2010/63/EU.

Compounds. SecinH3 (S7685), ML-7 (S8388), GW4896 (S7609), and Sotrastaurin (S2791) were purchased from Selleck Chemicals. A-740003 (HY-50697), and NAV-2729 (HY-112473) were purchased from MedChemExpress. ManumycinA (M6418) and ATP (A2383) were purchased from Sigma-Aldrich. SBFI-26 (AOnareB31865) was purchased from Aobious. PMA (10008014), (−)CP-55,940 (90084), Bradykinin (15539), (S)-3,5-DHPG (14411), 2-arachidonoyl glycerol, anandamide, AA, VDM11 (10006731), and OMDM-2 (10179) were purchased from Cayman Chemical. WOBE437 (80) and DH376 (63) were prepared in-house.

Biochemical and Cellular Studies. The $GRAB_{eCB2.0}$-based assay to study eCB release and transport using confocal microscopy and plate-based reader, as well as the EV isolation and characterization, targeted lipidomics, and proteomic analysis were performed as described in *SI Appendix, Supporting Experimental Procedures*.

Electrophysiology. Preparation of mouse brain slices and electrophysiological recordings were performed as described in *SI Appendix, Supporting Experimental Procedures*.

Mathematical Modeling. A semimechanistic mathematical model based on ordinary differential equations was developed to capture the signal formation dynamics of the Neuro2a-GRAB 2-AG signaling system as described in *SI Appendix, Supporting Text*. The model included the production, metabolism, and accumulation of 2-AG in Neuro2A cells, as well as its release into the extracellular space, and was fitted to the available time course fluorescence signal, while fixing several separately determined model parameters. Mixed-effects modeling was used to account for variability in fluorescence signal between wells associated with cell densities. Model fitting and simulations were performed using R (version 4.2.1).

Statistical Analysis. Statistical analysis was done in GraphPad Prism 8.4.3 or 9.0.0 as stated in the respective figure legends.

Data, Materials, and Software Availability. The code used to perform the model-based analysis presented in the manuscript can be found via GitHub (https://github.com/sebastian-tandar/endocannabionoid2ag) (81). The mass spectrometry proteomics data have been deposited to the ProteomeXchange Consortium via the PRIDE partner repository with the dataset identifier PXD056498 (82). All other data are included in the manuscript and/or *SI Appendix*.

ACKNOWLEDGMENTS. We thank the Netherlands Organization for Scientific Research VICI-grant, 724.017.002 (M.v.d.S.), and Frontier Program KKP129961 (I.K.) and NIH grant P30DA056410 (I.K.). Jeroen Punt and Mirjam Huizenga are acknowledged for their help in characterizing the molecular profile of SecinH3 and NAV2729.

Author affiliations: [a]Department of Molecular Physiology, Leiden University, Leiden 2333 CC, The Netherlands; [b]Department of Psychological and Brain Sciences, Indiana University Bloomington, Bloomington, IN 47405-2204; [c]Division of Systems Pharmacology & Pharmacy, Leiden Academic Centre for Drug Research, Leiden University, Leiden 2333 CC, The Netherlands; [d]Department of Medicinal Chemistry, Leiden University, Leiden 2333 CC, The Netherlands; [e]Oncode Institute, Leiden 2333 CC, The Netherlands; [f]State Key Laboratory of Membrane Biology, Peking University School of Life Sciences, Beijing 100871, China; [g]IDG/McGovern Institute for Brain Research, Peking University, Beijing 100871, China; [h]Peking-Tsinghua Center for Life Sciences, New Cornerstone Science Laboratory, Academy for Advanced Interdisciplinary Studies, Beijing 100871, China; [i]Department of Pharmacology, School of Medicine, University of Washington, Seattle, WA 98195; and [j]Molecular Neurobiology Research Group, Hungarian Research Network, Institute of Experimental Medicine, Budapest H-1083, Hungary

Author contributions: V.M.S., B.B., S.T.T., N.S., J.G.C.v.H., I.K., and M.v.d.S. designed research; V.M.S., B.B., S.T.T., A.F.S., T.v.d.W., N.Z., J.R., and C.v.d.H. performed research; N.v.E., Y.L., and N.S. contributed new reagents/analytical tools; V.M.S., B.B., S.T.T., A.F.S., J.R., C.v.d.H., L.H.H., Y.L., N.S., J.G.C.v.H., I.K., and M.v.d.S. analyzed the data; V.M.S., B.B., S.T.T., A.F.S., J.R., C.v.d.H., L.H.H., Y.L., N.S., J.G.C.v.H., I.K., and M.v.d.S. interpreted the data; and V.M.S., B.B., S.T.T., N.S., I.K., and M.v.d.S wrote the paper.

1. T. C. Südhof, Neurotransmitter release: The last millisecond in the life of a synaptic vesicle. *Neuron* **80**, 675–690 (2013).
2. D. Piomelli, G. Astarita, R. Rapaka, A neuroscientist's guide to lipidomics. *Nat. Rev. Neurosci.* **8**, 743–754 (2007).
3. B. E. Alger, J. Kim, Supply and demand for endocannabinoids. *Trends Neurosci.* **34**, 304–315 (2011).
4. G. Marsicano *et al.*, CB1 cannabinoid receptors and on-demand defense against excitotoxicity. *Science* **302**, 84–88 (2003).
5. A. C. Kreitzer, W. G. Regehr, Retrograde inhibition of presynaptic calcium influx by endogenous cannabinoids at excitatory synapses onto Purkinje cells. *Neuron* **29**, 717–727 (2001).
6. R. I. Wilson, R. A. Nicoll, Endogenous cannabinoids mediate retrograde signalling at hippocampal synapses. *Nature* **410**, 588–592 (2001).
7. M. Kano, T. Ohno-Shosaku, Y. Hashimotodani, M. Uchigashima, M. Watanabe, Endocannabinoid-mediated control of synaptic transmission. *Physiol. Rev.* **89**, 309–380 (2009).
8. A. Tanimura *et al.*, The endocannabinoid 2-arachidonoylglycerol produced by diacylglycerol lipase α mediates retrograde suppression of synaptic transmission. *Neuron* **65**, 320–327 (2010).
9. Y. Gao *et al.*, Loss of retrograde endocannabinoid signaling and reduced adult neurogenesis in diacylglycerol lipase knock-out mice. *J. Neurosci.* **30**, 2017–2024 (2010).
10. N. van Egmond, V. M. Straub, M. van der Stelt, Targeting endocannabinoid signaling: FAAH and MAG lipase inhibitors. *Annu. Rev. Pharmacol. Toxicol.* **61**, 441–463 (2021).

11. M. Maccarrone *et al.*, Goods and bads of the endocannabinoid system as a therapeutic target: Lessons learned after 30 years. *Pharmacol. Rev.* **75**, 885–958 (2023).
12. M. P. Baggelaar, M. Maccarrone, M. van der Stelt, 2-Arachidonoylglycerol: A signaling lipid with manifold actions in the brain. *Prog. Lipid Res.* **71**, 1–17 (2018).
13. K. M. Jung *et al.*, A key role for diacylglycerol lipase-α in metabotropic glutamate receptor-dependent endocannabinoid mobilization. *Mol. Pharmacol.* **72**, 612–621 (2007).
14. B. C. Shonesy *et al.*, CaMKII regulates diacylglycerol lipase-α and striatal endocannabinoid signaling. *Nat. Neurosci.* **16**, 456–463 (2013).
15. B. C. Shonesy, J. R. Stephenson, C. R. Marks, R. J. Colbran, Cyclic AMP–dependent protein kinase and D1 dopamine receptors regulate diacylglycerol lipase-α and synaptic 2-arachidonoyl glycerol signaling. *J. Neurochem.* **153**, 334–345 (2020).
16. D. R. Powell *et al.*, Diacylglycerol lipase α knockout mice demonstrate metabolic and behavioral phenotypes similar to those of cannabinoid receptor 1 knockout mice. *Front. Endocrinol.* **6**, 86 (2015).
17. I. Jenniches *et al.*, Anxiety, stress, and fear response in mice with reduced endocannabinoid levels. *Biol. Psychiatry* **79**, 858–868 (2016).
18. B. C. Shonesy *et al.*, Genetic disruption of 2-arachidonoylglycerol synthesis reveals a key role for endocannabinoid signaling in anxiety modulation. *Cell Rep.* **9**, 1644–1653 (2014).
19. M. Beltramo *et al.*, Functional role of high-affinity anandamide transport, as revealed by selective inhibition. *Science* **277**, 1094–1097 (1997).
20. C. J. Fowler, Transport of endocannabinoids across the plasma membrane and within the cell. *FEBS J.* **280**, 1895–1904 (2013).
21. J. L. Blankman, G. M. Simon, B. F. Cravatt, A comprehensive profile of brain enzymes that hydrolyze the endocannabinoid 2-arachidonoylglycerol. *Chem. Biol.* **14**, 1347–1356 (2007).
22. J. Z. Long *et al.*, Selective blockade of 2-arachidonoylglycerol hydrolysis produces cannabinoid behavioral effects. *Nat. Chem. Biol.* **5**, 37–44 (2009).
23. B. Pan *et al.*, Blockade of 2-arachidonoylglycerol hydrolysis by selective monoacylglycerol lipase inhibitor 4-nitrophenyl 4-(dibenzo[d][1,3]dioxol-5-yl(hydroxy)methyl)piperidine-1-carboxylate (JZL184) enhances retrograde endocannabinoid signaling. *J. Pharmacol. Exp. Ther.* **331**, 591–597 (2009).
24. S. G. Kinsey *et al.*, Blockade of endocannabinoid-degrading enzymes attenuates neuropathic pain. *J. Pharmacol. Exp. Ther.* **330**, 902–910 (2009).
25. N. R. Sciolino, W. Zhou, A. G. Hohmann, Enhancement of endocannabinoid signaling with JZL184, an inhibitor of the 2-arachidonoylglycerol hydrolyzing enzyme monoacylglycerol lipase, produces anxiolytic effects under conditions of high environmental aversiveness in rats. *Pharmacol. Res.* **64**, 226–234 (2011).
26. J. A. Noriega-Prieto *et al.*, Distinct endocannabinoids specifically signal to astrocytes and neurons. bioRxiv [Preprint] (2023). http://www.biorxiv.org/content/10.1101/2023.06.13.544877v1 (Accessed 13 March 2024).
27. A. Chicca *et al.*, Chemical probes to potently and selectively inhibit endocannabinoid cellular reuptake. *Proc. Natl. Acad. Sci. U.S.A.* **114**, E5006–E5015 (2017).
28. A. Dong *et al.*, A fluorescent sensor for spatiotemporally resolved imaging of endocannabinoid dynamics in vivo. *Nat. Biotechnol.* **40**, 787–798 (2022).
29. J. S. Farrell *et al.*, In vivo endocannabinoid dynamics at the timescale of physiological and pathological neural activity. *Neuron* **109**, 2398–2403.e4 (2021).
30. D. J. Liput *et al.*, 2-Arachidonoylglycerol mobilization following brief synaptic stimulation in the dorsal lateral striatum requires glutamatergic and cholinergic neurotransmission. *Neuropharmacology* **205**, 108916 (2022).
31. E. Albarran *et al.*, Postsynaptic synucleins mediate endocannabinoid signaling. *Nat. Neurosci.* **26**, 997–1007 (2023).
32. S. M. Augustin, A. L. Gracias, G. Luo, R. C. Anumola, D. M. Lovinger, Striatonigral direct pathway 2-arachidonoylglycerol contributes to ethanol effects on synaptic transmission and behavior. *Neuropsychopharmacology* **48**, 1941–1951 (2023).
33. S. Singh *et al.*, $P2X_7$ receptor–dependent increase in endocannabinoid 2-arachidonoyl glycerol production by neuronal cells in culture: Dynamics and mechanism. *Br. J. Pharmacol.* **181**, 2459–2477 (2024).
34. Y. Zhou *et al.*, Regulated endosomal trafficking of diacylglycerol lipase alpha (DAGLα) generates distinct cellular pools; implications for endocannabinoid signaling. *Mol. Cell. Neurosci.* **76**, 76–86 (2016).
35. A. Chicca, J. Marazzi, S. Nicolussi, J. Gertsch, Evidence for bidirectional endocannabinoid transport across cell membranes. *J. Biol. Chem.* **287**, 34660–34682 (2012).
36. V. Di Marzo *et al.*, Formation and inactivation of endogenous cannabinoid anandamide in central neurons. *Nature* **372**, 686–691 (1994).
37. G. Ortar, A. Ligresti, L. De Petrocellis, E. Morera, V. Di Marzo, Novel selective and metabolically stable inhibitors of anandamide cellular uptake. *Biochem. Pharmacol.* **65**, 1473–1481 (2003).
38. L. De Petrocellis, T. Bisogno, J. B. Davis, R. G. Pertwee, V. Di Marzo, Overlap between the ligand recognition properties of the anandamide transporter and the VR1 vanilloid receptor: Inhibitors of anandamide uptake with negligible capsaicin-like activity. *FEBS Lett.* **483**, 52–56 (2000).
39. M. Kaczocha, S. T. Glaser, D. G. Deutsch, Identification of intracellular carriers for the endocannabinoid anandamide. *Proc. Natl. Acad. Sci. U.S.A.* **106**, 6375–6380 (2009).
40. B. Sanson *et al.*, Crystallographic study of FABP5 as an intracellular endocannabinoid transporter. *Acta Crystallogr. D Biol. Crystallogr.* **70**, 290–298 (2014).
41. S. Haj-Dahmane *et al.*, Fatty-acid-binding protein 5 controls retrograde endocannabinoid signaling at central glutamate synapses. *Proc. Natl. Acad. Sci. U.S.A.* **115**, 3482–3487 (2018).
42. M. Fauzan *et al.*, Fatty acid–binding protein 5 modulates brain endocannabinoid tone and retrograde signaling in the striatum. *Front. Cell. Neurosci.* **16**, 936939 (2022).
43. Y. Zhou *et al.*, Identification of fatty acid binding protein 5 inhibitors through similarity-based screening. *Biochemistry* **58**, 4304–4316 (2019).
44. F. Bianco *et al.*, Acid sphingomyelinase activity triggers microparticle release from glial cells. *EMBO J.* **28**, 1043–1054 (2009).
45. M. Gabrielli *et al.*, Active endocannabinoids are secreted on extracellular membrane vesicles. *EMBO Rep.* **16**, 213–220 (2015).
46. M. Lombardi *et al.*, Extracellular vesicles released by microglia and macrophages carry endocannabinoids which foster oligodendrocyte differentiation. *Front. Immunol.* **15**, 1331210 (2024).
47. Y. Nakamura *et al.*, Cocaine-induced endocannabinoid signaling mediated by sigma-1 receptors and extracellular vesicle secretion. *Elife* **8**, e47209 (2019).
48. M. Catalano, L. O'Driscoll, Inhibiting extracellular vesicles formation and release: A review of EV inhibitors. *J. Extracell. Vesicles* **9**, 1703244 (2020).
49. V. Muralidharan-Chari *et al.*, ARF6-regulated shedding of tumor cell–derived plasma membrane microvesicles. *Curr. Biol.* **19**, 1875–1885 (2009).
50. M. Saitoh, T. Ishikawa, S. Matsushima, M. Naka, H. Hidaka, Selective inhibition of catalytic activity of smooth muscle myosin light chain kinase. *J. Biol. Chem.* **262**, 7796–7801 (1987).
51. S. Singh *et al.*, ABHD6 selectively controls metabotropic-dependent increases in 2-AG production. bioRxiv [Preprint] (2022). http://www.biorxiv.org/content/10.1101/2022.05.18.492553v2 (Accessed 2 September 2024).
52. I. Vetter, R. J. Lewis, Characterization of endogenous calcium responses in neuronal cell lines. *Biochem. Pharmacol.* **79**, 908–920 (2010).
53. Y. Ikeda, A. Ueno, H. Naraba, N. Matsuki, S. Oh-ishi, Intracellular Ca2+ increase in Neuro-2A cells and rat astrocytes following stimulation of bradykinin B2 receptor. *Jpn. J. Pharmacol.* **84**, 140–145 (2000).
54. Y. Hashimotodani, T. Ohno-Shosaku, M. Kano, Presynaptic monoacylglycerol lipase activity determines basal endocannabinoid tone and terminates retrograde endocannabinoid signaling in the hippocampus. *J. Neurosci.* **27**, 1211–1219 (2007).
55. D. Sun, Y. Guo, P. Tang, H. Li, L. Chen, Arf6 as a therapeutic target: Structure, mechanism, and inhibitors. *Acta Pharm. Sin. B* **13**, 4089–4104 (2023).
56. J. Li *et al.*, Serum-free culture alters the quantity and protein composition of neuroblastoma-derived extracellular vesicles. *J. Extracell. Vesicles* **4**, 1–12 (2015).
57. J. Taylor, R. Jaiswal, M. Bebawy, Calcium-calpain dependent pathways regulate vesiculation in malignant breast cells. *Curr. Cancer Drug Targets* **17**, 486–494 (2017).
58. H. T. McMahon, E. Boucrot, Membrane curvature at a glance. *J. Cell Sci.* **128**, 1065–1070 (2015).
59. H. Pollet, L. Conrard, A.-S. Cloos, D. Tyteca, Plasma membrane lipid domains as platforms for vesicle biogenesis and shedding? *Biomolecules* **8**, 94 (2018).
60. M. Chivet *et al.*, Exosomes secreted by cortical neurons upon glutamatergic synapse activation specifically interact with neurons. *J. Extracell. Vesicles* **3**, 24722 (2014).
61. G. Lachenal *et al.*, Release of exosomes from differentiated neurons and its regulation by synaptic glutamatergic activity. *Mol. Cell. Neurosci.* **46**, 409–413 (2011).
62. J. W. Clancy, M. Schmidtmann, C. D'Souza-Schorey, The ins and outs of microvesicles. *FASEB BioAdv.* **3**, 399–406 (2021).
63. D. Ogasawara *et al.*, Rapid and profound rewiring of brain lipid signaling networks by acute diacylglycerol lipase inhibition. *Proc. Natl. Acad. Sci. U.S.A.* **113**, 26–33 (2016).
64. T. Sakuragi, S. Nagata, Regulation of phospholipid distribution in the lipid bilayer by flippases and scramblases. *Nat. Rev. Mol. Cell Biol.* **24**, 576–596 (2023).
65. T. Bisogno *et al.*, The uptake by cells of 2-arachidonoylglycerol, an endogenous agonist of cannabinoid receptors. *Eur. J. Biochem.* **268**, 1982–1989 (2001).
66. A. Ligresti *et al.*, Exploiting nanotechnologies and TRPV1 channels to investigate the putative anandamide membrane transporter. *PLoS One* **5**, e10239 (2010).
67. J. W. Clancy *et al.*, Regulated delivery of molecular cargo to invasive tumour-derived microvesicles. *Nat. Commun.* **6**, 6919 (2015).
68. C. Liu *et al.*, Identification of the SNARE complex that mediates the fusion of multivesicular bodies with the plasma membrane in exosome secretion. *J. Extracell. Vesicles* **12**, 12356 (2023).
69. Y. Hu *et al.*, Microparticles: Biogenesis, characteristics and intervention therapy for cancers in preclinical and clinical research. *J. Nanobiotechnol.* **20**, 189 (2022).
70. L. R. Lizarraga-Valderrama, G. K. Sheridan, Extracellular vesicles and intercellular communication in the central nervous system. *FEBS Lett.* **595**, 1391–1410 (2021).
71. A. Montecalvo *et al.*, Mechanism of transfer of functional microRNAs between mouse dendritic cells via exosomes. *Blood* **119**, 756–766 (2012).
72. Z. H. Kwok, C. Wang, Y. Jin, Extracellular vesicle transportation and uptake by recipient cells: A critical process to regulate human diseases. *Processes* **9**, 273 (2021).
73. Y. Chen *et al.*, Neuronal and astrocytic monoacylglycerol lipase limit the spread of endocannabinoid signaling in the cerebellum. *eNeuro* **3**, ENEURO.0048-16.2016 (2016).
74. A. Straiker *et al.*, Monoacylglycerol lipase limits the duration of endocannabinoid-mediated depolarization-induced suppression of excitation in autaptic hippocampal neurons. *Mol. Pharmacol.* **76**, 1220–1227 (2009).
75. A. K. Sharma, R. Khandelwal, C. Wolfrum, Futile lipid cycling: From biochemistry to physiology. *Nat. Metab.* **6**, 808–824 (2024).
76. R. Nyilas *et al.*, Enzymatic machinery for endocannabinoid biosynthesis associated with calcium stores in glutamatergic axon terminals. *J. Neurosci.* **28**, 1058–1063 (2008).
77. M. van der Stelt *et al.*, Anandamide acts as an intracellular messenger amplifying Ca2+ influx via TRPV1 channels. *EMBO J.* **24**, 3026–3037 (2005).
78. M. A. Nolte, E. N. M. Nolte-'t Hoen, C. Margadant, Integrins control vesicular trafficking; new tricks for old dogs. *Trends Biochem. Sci.* **46**, 124–137 (2021).
79. T. Yoshida *et al.*, Localization of diacylglycerol lipase-α around postsynaptic spine suggests close proximity between production site of an endocannabinoid, 2-arachidonoyl-glycerol, and presynaptic cannabinoid CB1 receptor. *J. Neurosci.* **26**, 4740–4751 (2006).
80. B. Gagestein *et al.*, Chemical proteomics reveals off-targets of the anandamide reuptake inhibitor WOBE437. *ACS Chem. Biol.* **17**, 1174–1183 (2022).
81. S. T. Tandar, endocannabionoid2ag. Github. https://github.com/sebastian-tandar/endocannabionoid2ag. Deposited 30 September 2024.
82. V. M. Straub *et al.*, The endocannabinoid 2-arachidonoylglycerol is released and transported on demand via extracellular microvesicles. PRIDE Proteomics Identifications Database. https://www.ebi.ac.uk/pride/archive/projects/PXD056498. Deposited 4 October 2024.